Supporting Information

Additive-free selective oxidation of aromatic alcohols with molecular oxygen catalyzed by a mixed-valence polyoxovanadate-based metal–organic framework

Hongrui Tian,[†, a] Runhan Li,[†, b] Jun Miao,[a] Shuxia Liu,[c] Fengfeng Wang[d] & Zhiping Zheng*,[a]

[a] Department of Chemistry and Shenzhen Grubbs Institute, Southern University of Science and Technology, Shenzhen, Guangdong 518055, China.

[b] School of Chemistry, South China Normal University, Guangzhou, Guangdong 510006, China

[c] Key Laboratory of Polyoxometalate and Reticular Material Chemistry of Ministry of Education, College of Chemistry, Northeast Normal University, Ren Min Street No. 5268, Changchun, Jilin 130024, P. R. China

[d] National Institutes for Food and Drug Control, 31 Huatuo Road, Daxing District, Beijing, 102600, China.

Corresponding author E-mail: *zhengzp@sustech.edu.cn*

[†]   These   authors   contributed   equally.

Table of Contents

1. Computational details

Methods

All of the potential energy surface calculations were performed with (U)B3LYP-D3(BJ) functional. Full ground-state geometry optimizations were carried out at the SMD(acetonitrile)/(U)B3LYP-D3/Def2-SVP[1] level. Frequencies were calculated at the same theoretical level to verify the stationary points to be equilibriums or be transition states. Intrinsic reaction coordinate[2] (IRC) calculations were carried out to ensure the correct transition states connecting reactants and products. A better basis set system was employed to evaluate the single-point energy at the the SMD(acetonitrile)/(U)B3LYP-D3/Def2-TZVP[3] level, and combined it with the gas phase Gibbs free energy corrected by the thermodynamic energy (see below) to assess the free energy at 393.15 K and 0.8 Mpa in this work. All of the above calculations were performed with Gaussian 09 program.

Correction of translational entropy in solution

We evaluated the electronic energy (Esol) with zero-point energy correction in solution. For each species, the Esol is defined through equation:

$$E_{sol} = E_{sol}^{pot} + E_{gas}^{v_0}$$

where E_{sol}^{pot} is the potential energy including non-electrostatic energy in solution and $E_{gas}^{v_0}$ represents the zero-point vibrational energy in the gas phase. In a bimolecular

process, such as the radical capture or dissociation, the entropy change must be taken into consideration because the entropy considerably decreases or increases.

In this case, Gibbs energy (G_{sol}^o) is evaluated as follows:

$$G_{sol}^o = H_0 - T\left(S_r^o + S_v^o + S_t^o\right)$$

$$= E^T + P\Delta V - T\left(S_r^o + S_v^o + S_t^o\right)$$

$$= E_{sol} + E_{therm} - T\left(S_r^o + S_v^o + S_t^o\right)$$

where ΔV is 0 in solution, E_{therm} is the thermal correction by translational, vibrational, and rotational movement, and S_r^o, S_v^o, and S_t^o are rotational, vibrational, and translational entropies, respectively. In general, the Sackur-Tetrode equation is used to evaluate translational entropy S_t^o. In solution, however, the usual Sackur-Tetrode equation cannot be directly applied to the evaluation of S_t^o, because the translation movement is suppressed very much in solution. In this context, the translational entropy was corrected with the method developed by Whitesides et al.,[4] where the rotational entropy was evaluated in a normal manner. Thermal correction and entropy contributions of vibration movements to the Gibbs energy were evaluated with the frequencies calculated at 393.15 K and 0.8 MPa.

2. Crystallographic data and structure refinements

Table S1 Crystallographic data and structure refinement of **V-Cd-MOF**

Name	V-Cd-MOF
Empirical formula	$C_{98}H_{114}N_{28}O_{75}Cl_2V_{30}Cd$
Formula weight	4595.67
Temperature (K)	296
Wave length (Å)	0.71073
Crystal system	monoclinic
Space group	C2/c
a (Å)	46.762(3)
b (Å)	12.8284(9)
c (Å)	29.674(2)
α (deg)	90
β (deg)	121.786(2)
γ (deg)	90
Volume ($Å^3$)	15131.0(18)
Z, Dcalc (Mg/m^3)	4, 2.017
Absorption coefficient (mm^{-1})	2.028
F (000)	9080.0
Crystal size (mm^3)	$0.22 \times 0.21 \times 0.21$
θ range (deg)	4.416 to 0.17
index range (deg)	$-55 \le h \le 55, -15 \le k \le 15, -35 \le l \le 35$
Reflections collected / unique	82167 / 13417 [Rint = 0.1306]
Data / restraints / parameters	13417 / 66 / 1059
Goodness-of-fit on F^2	1.011
R1, wR_2 (I > 2σ(I))	0.0482, 0.0990
R1, wR_2 (all data)	0.0982, 0.1188
Largest diff. peak and hole (e $Å^{-3}$)	2.08, -0.56

$R_1 = \sum||F_o|-|F_c||/\sum|F_o| \cdot wR_2 = [\sum[w(F_o^2-F_c^2)^2]/\sum[w(F_o^2)^2]]^{1/2}$

## 3. PXRD patterns of V-Cd-MOF
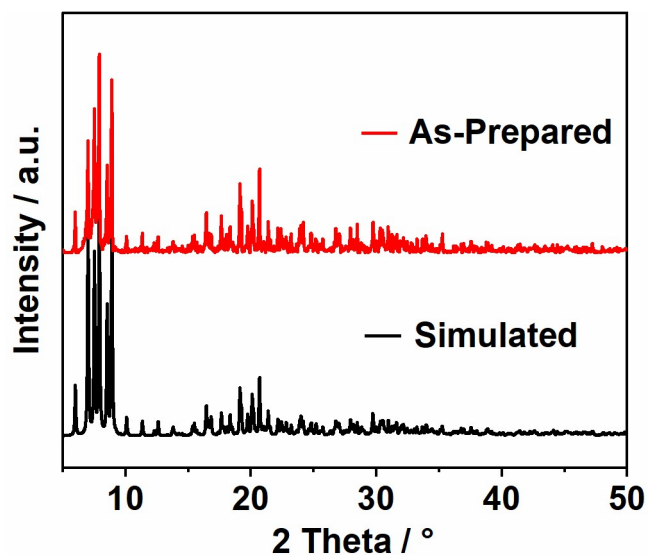
Fig. S1 The PXRD patterns of **V-Cd-MOF**.

## 4. FTIR spectrum of V-Cd-MOF
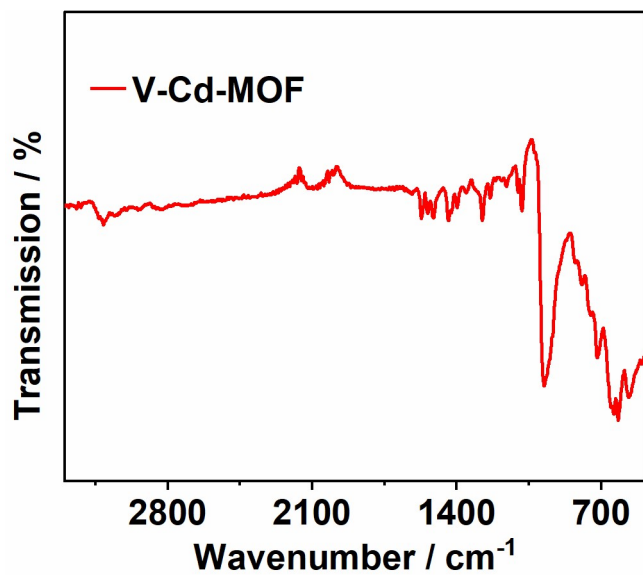
Fig. S2 The FTIR spectrum of **V-Cd-MOF**.

5. TGA curve of V-Cd-MOF
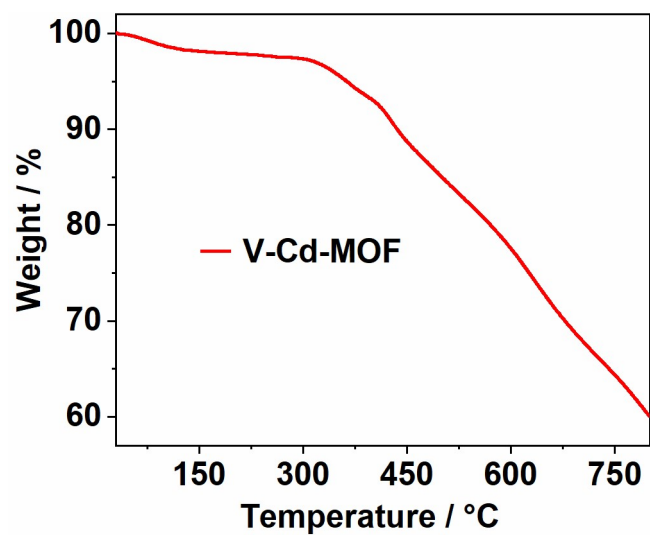

Fig. S3 The TGA curve of **V-Cd-MOF**.

6. The PXRD patterns of the V-Cd-MOF samples recovered after immersion
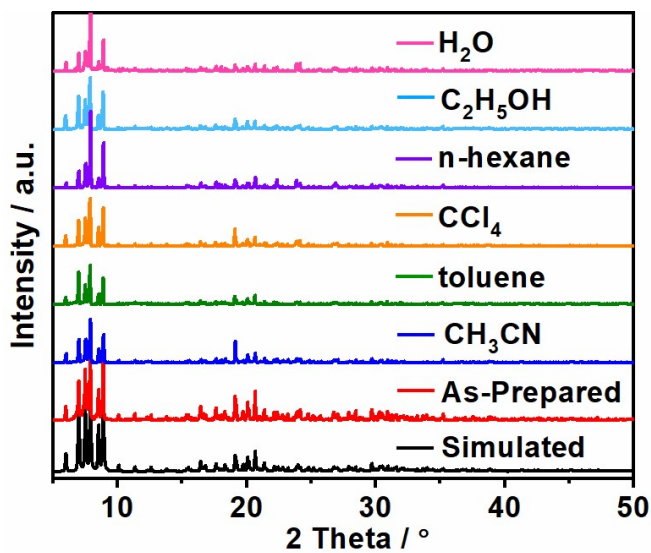
**Fig. S4** The PXRD patterns of the V-Cd-MOF samples recovered after solvent immersion at 120 ºC for 24 hours.

7. Protonated ligand [H₂bix]²⁺ in the V-Cd-MOF
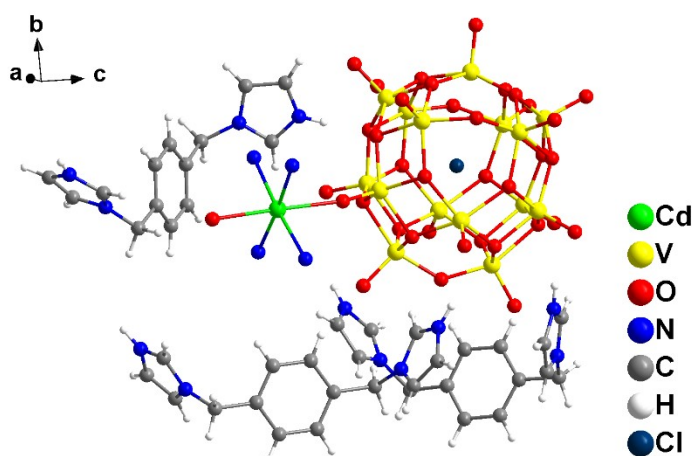
**Fig. S5** Protonated ligand $[H_2bix]^{2+}$ in the **V-Cd-MOF**.

## 8. The N₂ adsorption / desorption isotherms of V-Cd-MOF
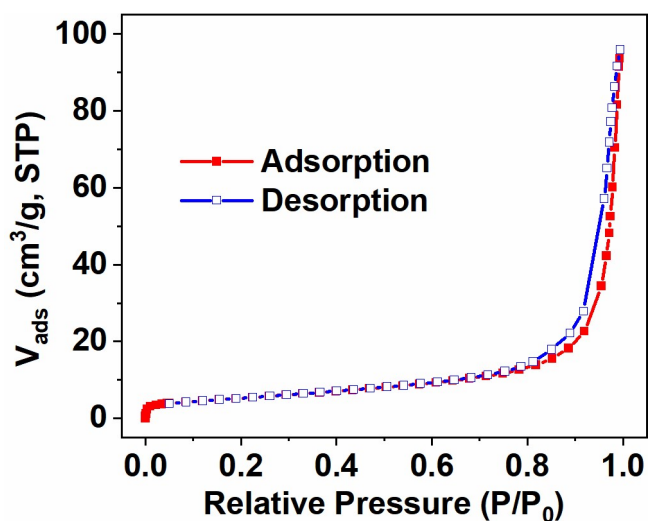
Fig. S6 The N₂ adsorption / desorption isotherms of **V-Cd-MOF** (measured at 77K, P_0 = 101 kPa).

9. The hydrogen bonds in the V-Cd-MOF

Table S2 The distance between non-hydrogen atoms in the hydrogen bond network of

V-Cd-MOF

Atoms involved	Length (Å)	Atoms involved	Length (Å)
N26⋯O7	2.970	N8⋯O36	2.906
N25⋯O15	2.750	N51⋯O16	3.214
N25⋯O11	3.193	N50⋯O11	2.941
N50⋯O30	2.907		

10. BVS results.

Table S3 BVS results for the vanadium ions and cadmium ions in **V-Cd-MOF**

Metal site	BVS cacl.	Assigned O.S.	Metal site	BVS cacl.	Assigned O.S.
Cd	2.11	2	V8	4.03	4
V1	4.39	4	V9	4.86	5
V2	4.48	4	V10	4.92	5
V3	4.50	4	V11	4.89	5
V4	4.10	4	V12	5.01	5
V5	4.82	5	V13	4.35	4
V6	4.38	4	V14	4.02	4
V7	4.79	5	V15	4.92	5

## 11. XPS spectra of V and Cd in V-Cd-MOF
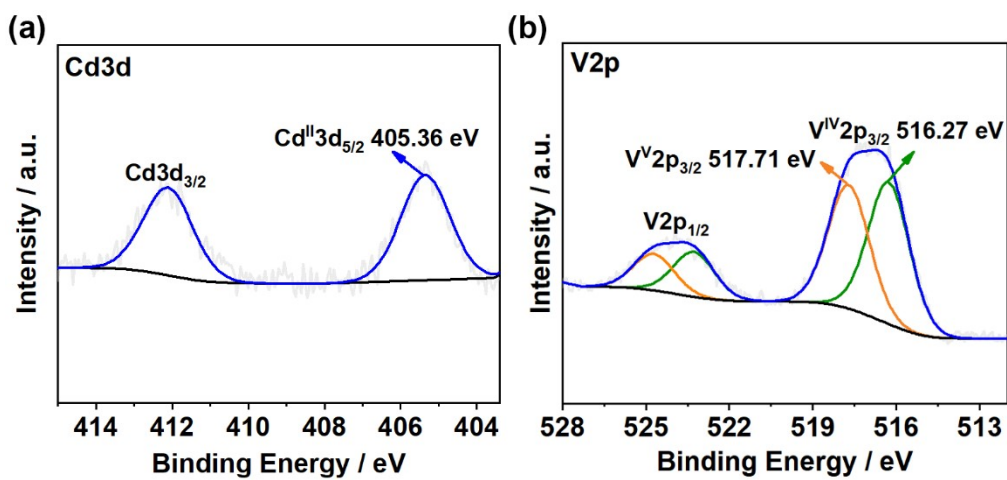
Fig. S7 XPS spectra of Cd and V in **V-Cd-MOF**.

12. TEM image of the ground V-Cd-MOF
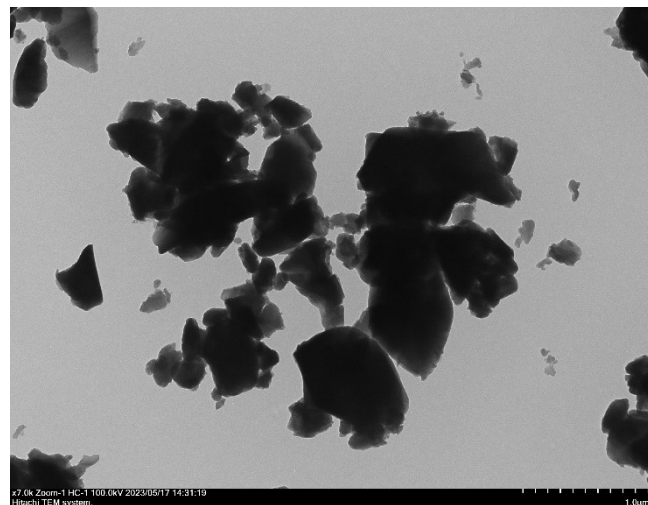
Fig. S8 TEM image of the ground **V-Cd-MOF**.

13. The influences of reaction conditions on the selective oxidation of BA to BAD
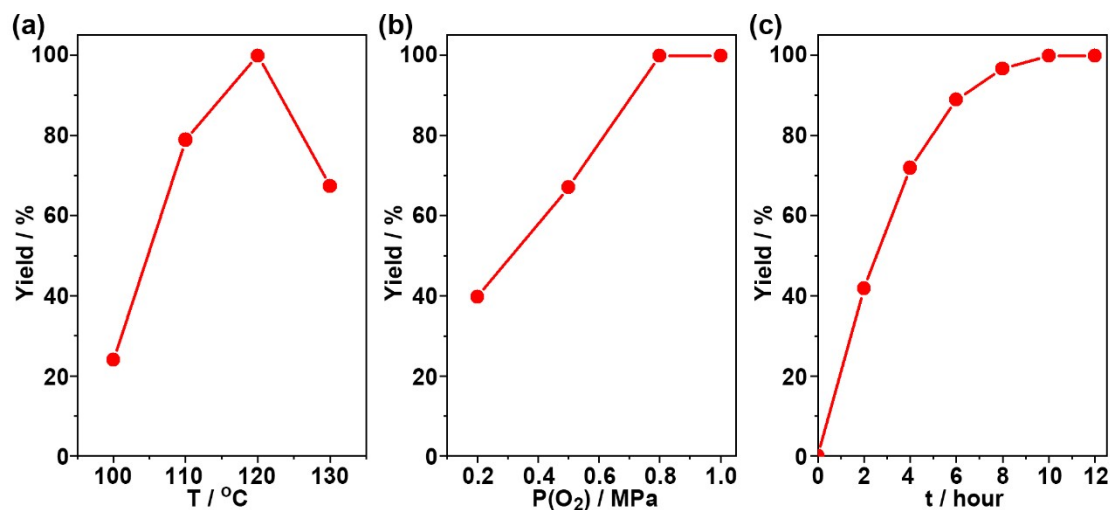
Fig. S9 The influences of reaction conditions on the selective oxidation of BA to BAD using the **V-Cd-MOF** as catalyst. (a) The effect of reaction temperature. (b) The effect of O_2 pressure. (c) The effect of reaction time. Reaction conditions: BA (0.5 mmol), **V-Cd-MOF** (0.005 mmol, 1% mol), 1-bromododecane (internal standard, 50 μL), CH_3CN (2 mL), O_2 (0.8 MPa) and at 120 °C for 10 hours. The yield was determined by GC analyses.

14. The solvent effect on the selective oxidation of BA to BAD
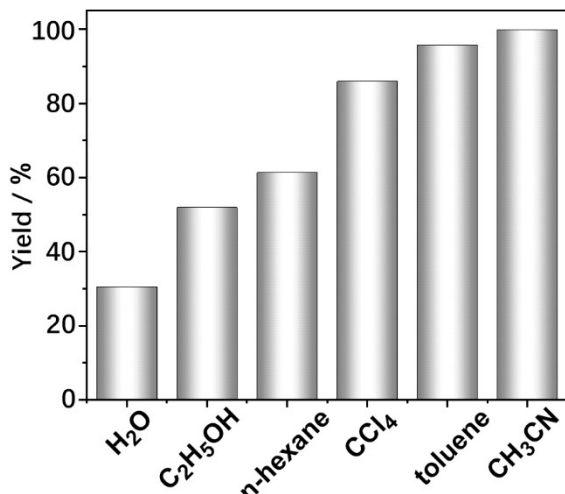
Fig. S10 The solvent effect on the selective oxidation of BA to BAD using the **V-Cd-MOF** as catalyst. Reaction conditions: BA (0.5 mmol), **V-Cd-MOF** (0.005 mmol, 1% mol), 1-bromododecane (internal standard, 50 μL), solvent (2 mL), O_2 (0.8 MPa) and at 120 °C for 10 hours. The yield was determined by GC analyses.

15. FTIR spectra and PXRD patterns of recovered V-Cd-MOF
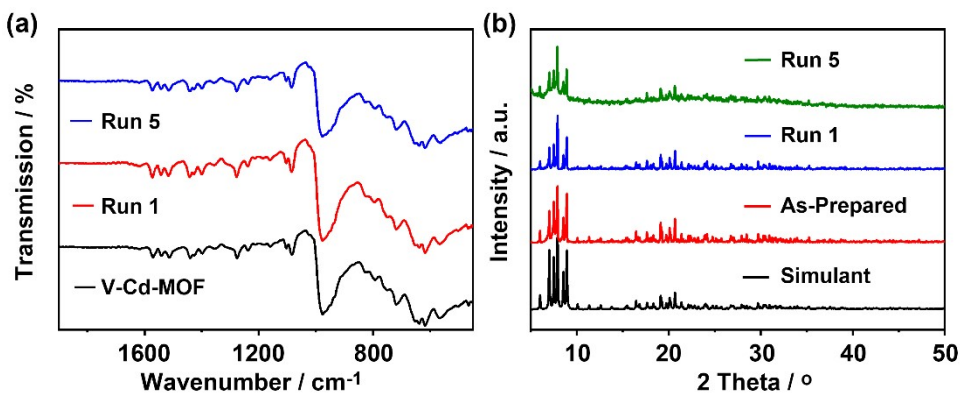
Fig. S11 (a) FTIR spectra of **V-Cd-MOF** before and after catalytic uses. (b) PXRD patterns of **V-Cd-MOF** before and after catalytic uses.

16. XPS spectra of recovered V-Cd-MOF
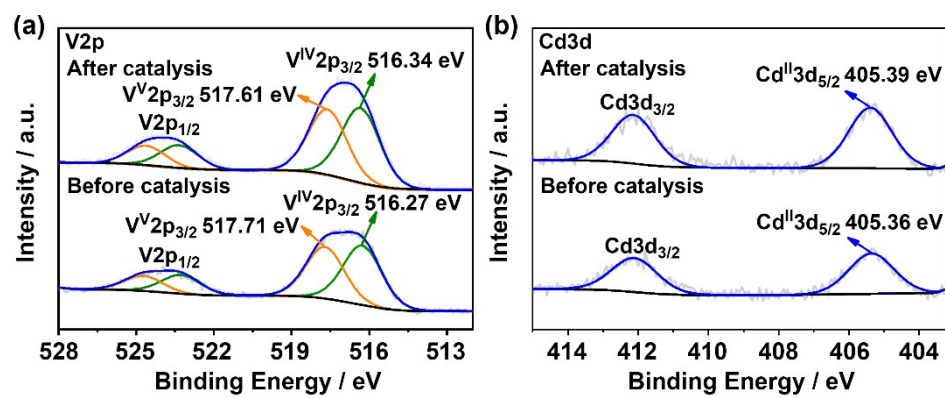
Fig. S12 XPS results of vanadium ions (a) and cadmium ions (b) of **V-Cd-MOF** before and after catalytic uses.

17. Comparison of different heterogeneous catalysts used for BA oxidation

Table S4 Comparison of different heterogeneous catalysts used for BA oxidation
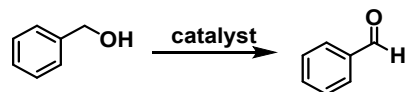
| entry	catalyst	oxidant	additive	conv. (%)	sel. (%)	TON	ref.
1	Cu(mIM)$_4$V$_2$O$_6$	H$_2$O$_2$	—	98.7	100	24.1	[5]
2	nano-γ-Fe$_2$O$_3$	H$_2$O$_2$	—	33	97	32.0	[6]
3	V/SiO$_2$	t-BuOOH	—	>99	>99	20.0	[7]
4	Co$_3$O$_4$/AC	O$_2$ (0.1 MPa)	—	100	87.3	3.1	[8]
5	Cu(BPYDCDE) (OAc)$_2$	Air	TEMPO	100	100	50	[9]
6	Cu$_3$(BTC)$_2$	O$_2$ (0.1 MPa)	TEMPO/ Na$_2$CO$_3$	>99	>99	3.7	[10]
7	Ni(OH)$_2$	O$_2$ (0.1 MPa)	—	98	100	0.3	[11]
8	**V-Cd-MOF**	O$_2$ (0.8 MPa)	—	>99	100	100	this work

Turnover number (TON) = mol of product / mol of catalyst

18. The coordination mode of Cd in Cd(Inic)$_2$ and the PXRD patterns of Cd(Inic)$_2$·0.5 DMF
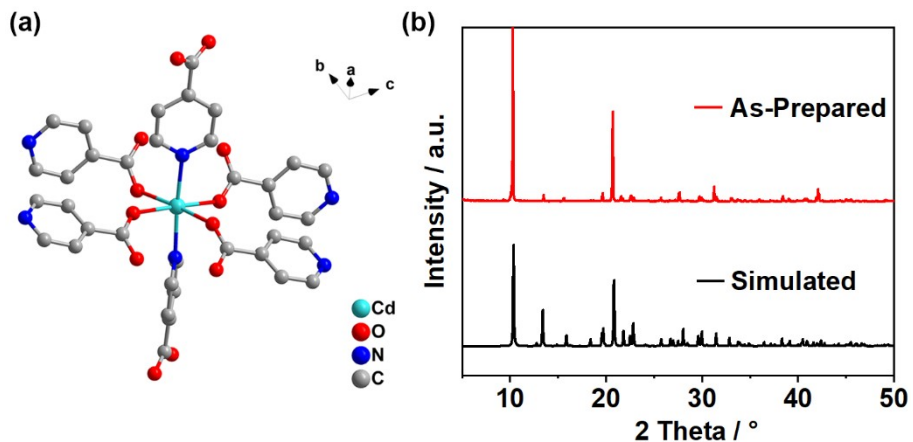
Fig. S13 (a) The coordination mode of Cd in Cd(Inic)$_2$. (b) The PXRD patterns of Cd(Inic)$_2$·0.5 DMF.

19. The structure of $\{V^{IV}_{16}V^{V}_{18}O_{82}\}^{10-}$ and the PXRD patterns of $K_{10}\{V^{IV}_{16}V^{V}_{18}O_{82}\}$·20H$_2$O
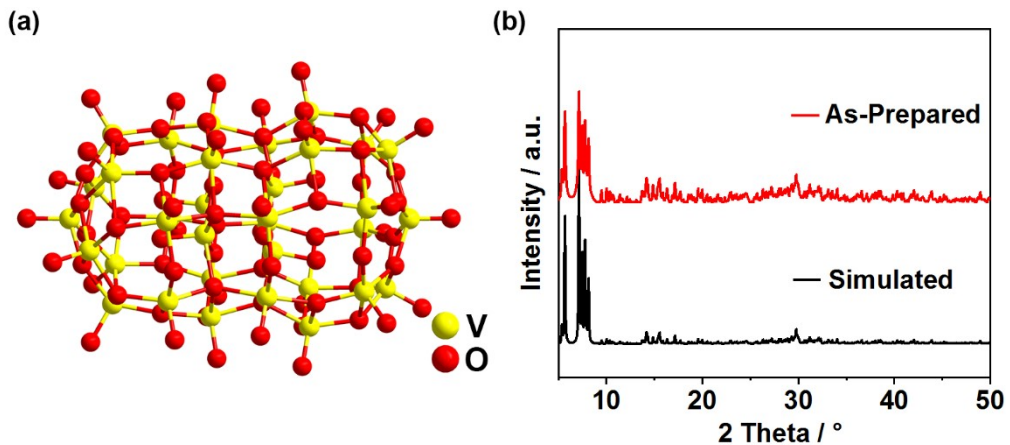
Fig. S14 (a) The structure of $\{V^{IV}_{16}V^{V}_{18}O_{82}\}^{10-}$. (b) The PXRD patterns of $K_{10}\{V^{IV}_{16}V^{V}_{18}O_{82}\}$·20H$_2$O (**MV-{V$_{34}$}**).

20. The structure of {V₁₆}-MOF and the PXRD patterns of the {V₁₆}-MOF
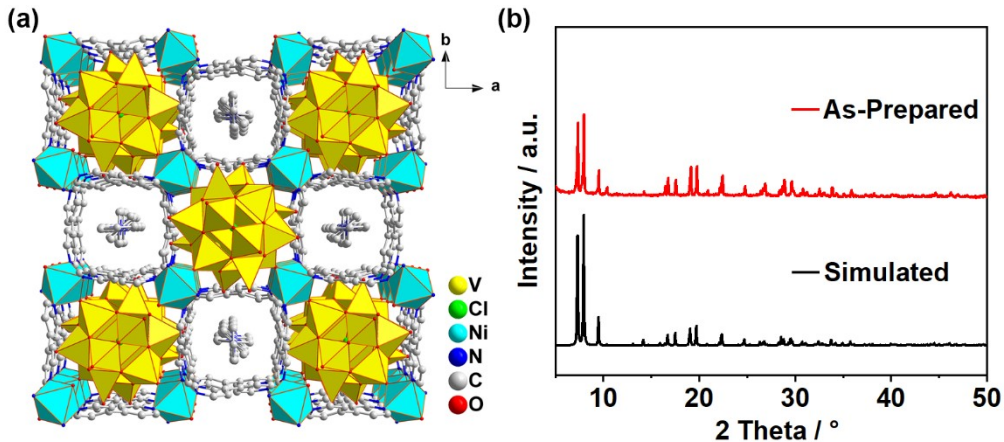
Fig. S15 (a) The structure of **{V₁₆}-MOF**. (b) The PXRD patterns of the **{V₁₆}-MOF**.

21. Structures of open-shell singlet and nonet {V₁₅} clusters

{V₁₅}$^{S=1}$
0.94 kcal/mol
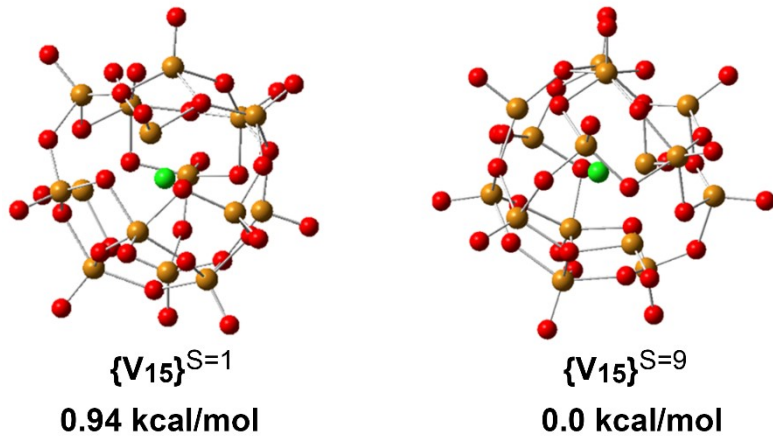
{V₁₅}$^{S=9}$
0.0 kcal/mol

Fig. S16 Structures of open-shell singlet and nonet **{V₁₅}** clusters. The Gibbs free energies are given in kcal/mol, relative to the most stable nonet **{V₁₅}**$^{S=9}$ conformation. To identify the stable catalytic activity species, we investigated the different spin states of the **{V₁₅}** clusters using unrestricted open-shell DFT at the same level, respectively. The nonet state **{V₁₅}** is proved more stable. (The **{V₁₅}** mentioned in this paper corresponded triplet **{V₁₅}**$^{S=9}$).

22. Assessing the possible conformation of a {V$_{15}$}-bound BA molecule

{V$_{15}$}-1
ΔE$_{ads}$ = 11.8

{V$_{15}$}-1a
ΔE$_{ads}$ = 72.7

{V$_{15}$}-1b
ΔE$_{ads}$ = 13.1

{V$_{15}$}-1c
ΔE$_{ads}$ = 29.3
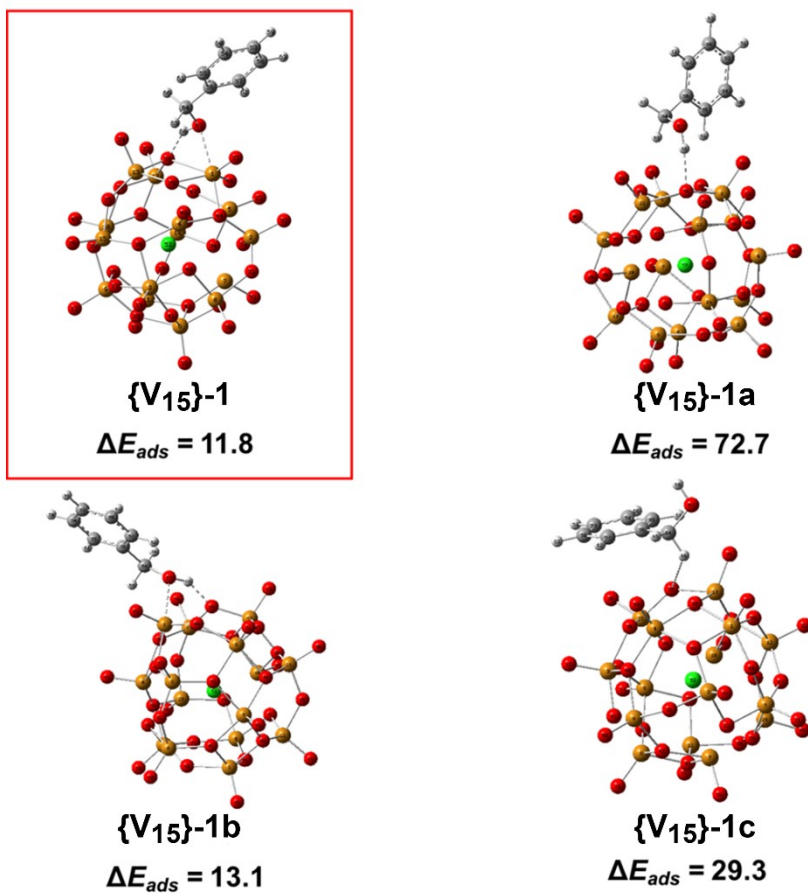
Fig. S17 Assessing the possible conformation of a {V$_{15}$}-bound BA molecule. The Gibbs free energies are given in kcal/mol. White, gray, red, green and yellow spheres represent H, C, O, Cl and V atoms, respectively.

23. ¹H-NMR spectra of the isolated aldehydes
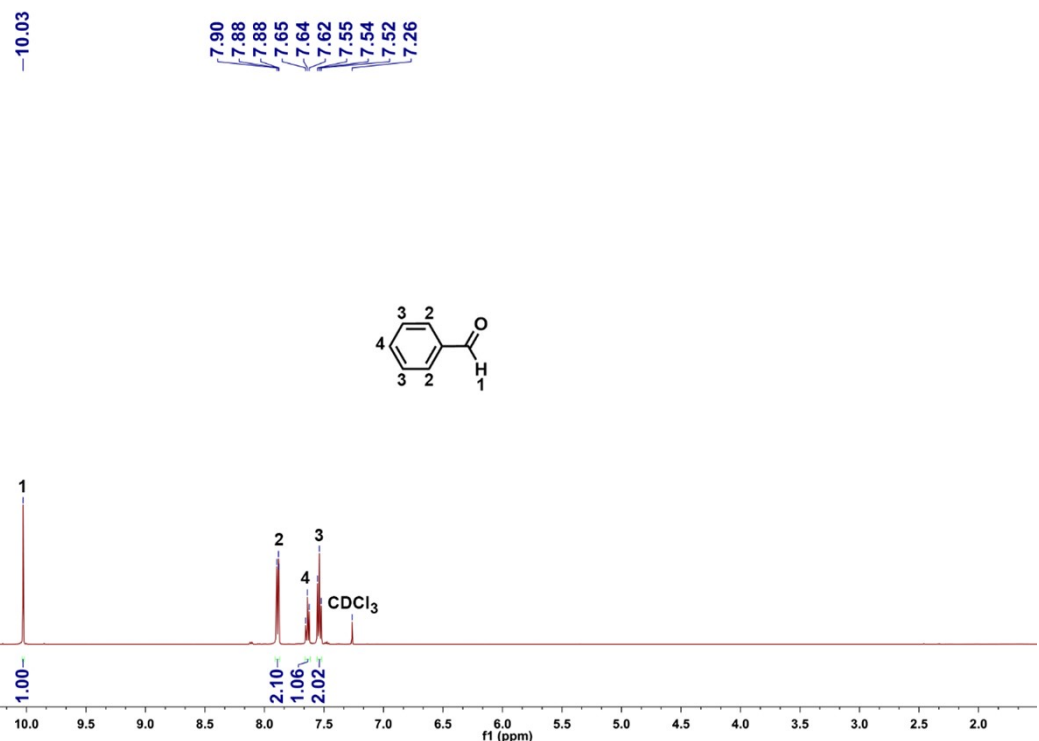
benzaldehyde. Light yellow oil. ¹H-NMR (400 MHz, CDCl₃).
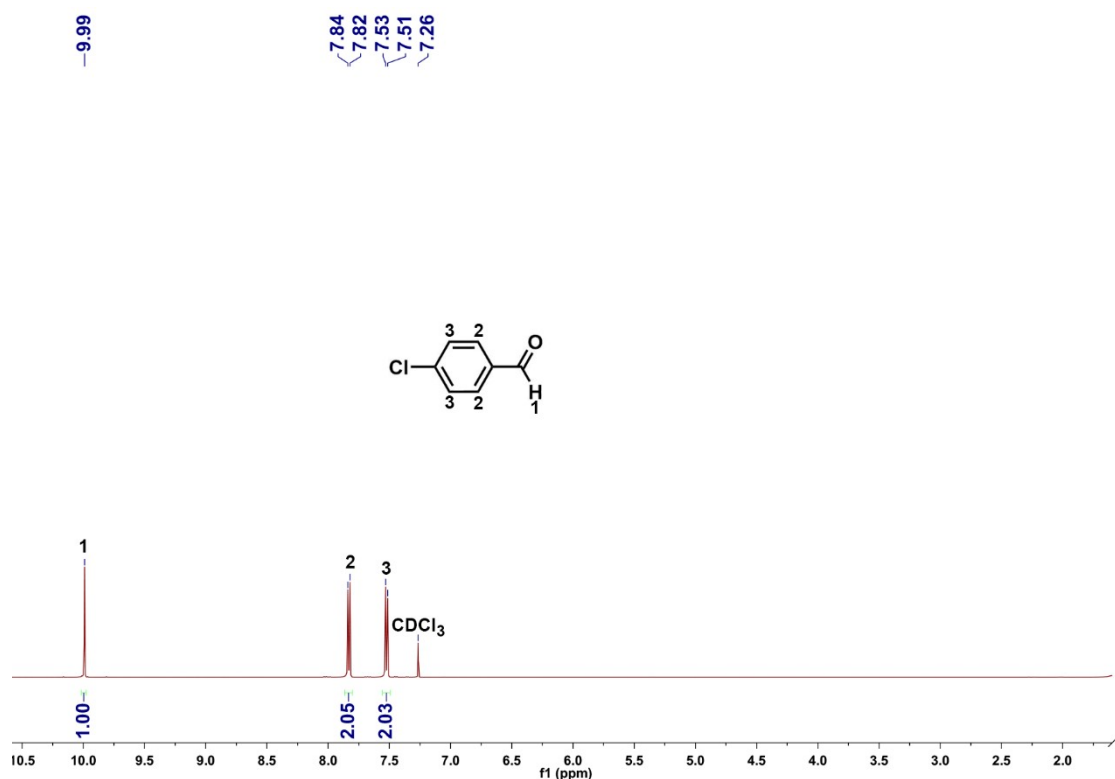
4-chlorobenzaldehyde. Light yellow solid. ¹H-NMR (400 MHz, CDCl₃).
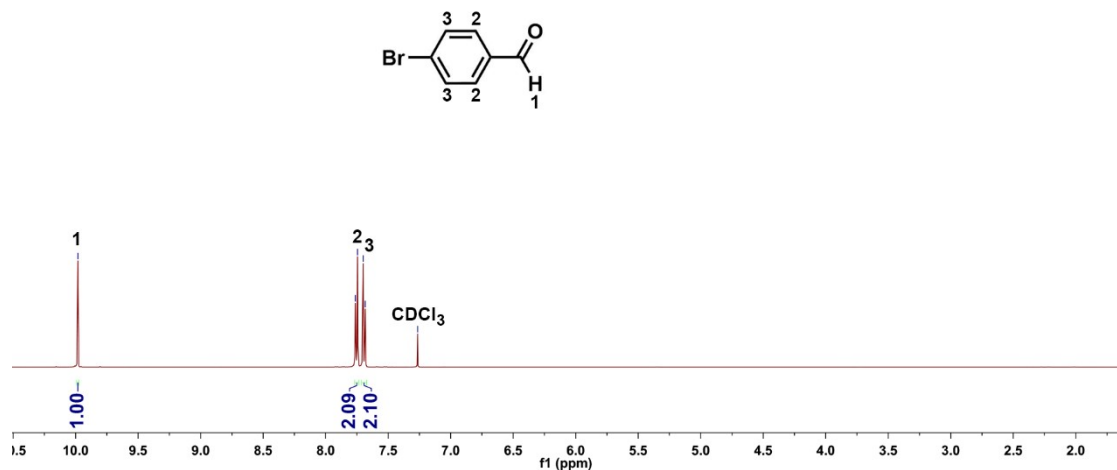
4-bromobenzaldehyde. Light yellow solid. ^{1}H-NMR (400 MHz, CDCl$_3$).
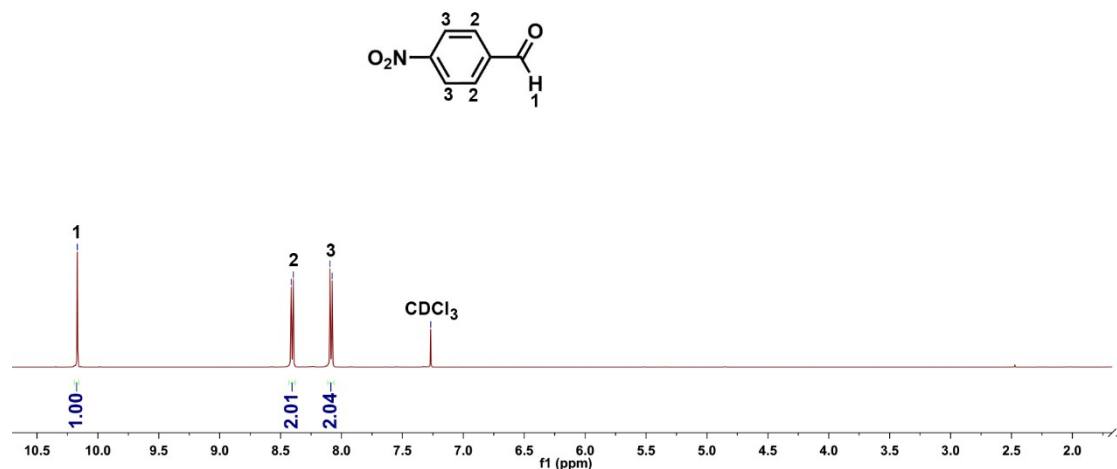
4-nitrobenzaldehyde. Yellow solid. ^{1}H-NMR (400 MHz, CDCl$_3$).
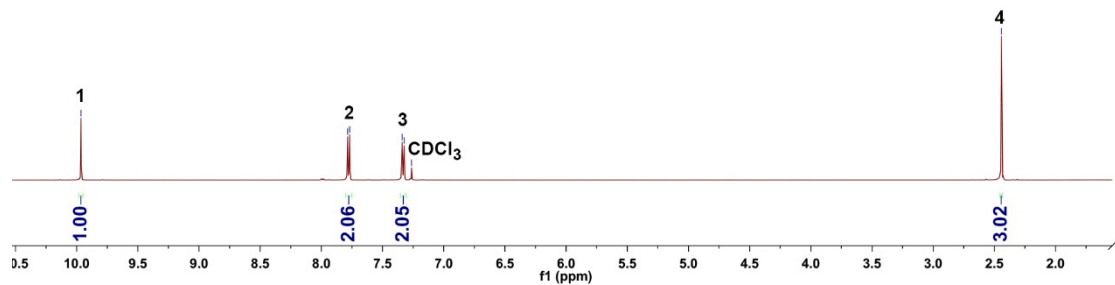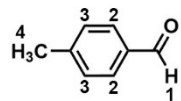
4-methylbenzaldehyde. Light yellow oil. ^{1}H-NMR (400 MHz, CDCl$_3$).
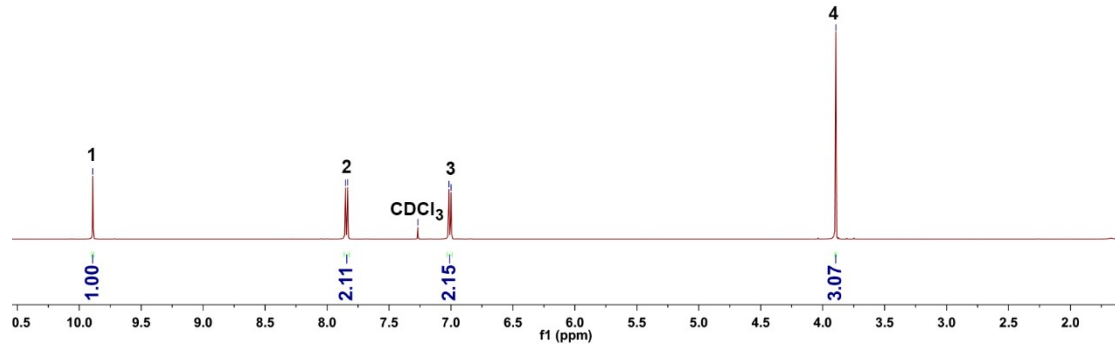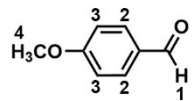
4-methoxybenzaldehyde. Light yellow oil. ^{1}H-NMR (400 MHz, CDCl$_3$).

9.67

7.70
7.28
7.27
7.26
6.62
6.62
6.61
6.61
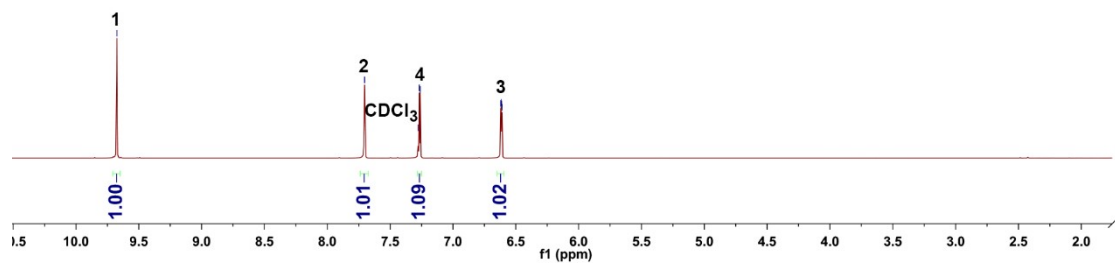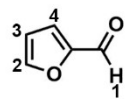
2-furaldehyde. Yellow oil. ^{1}H-NMR (400 MHz, CDCl$_3$).

10.06
7.97
7.95
7.77
7.77
7.75
7.75
7.66
7.65
7.65
7.63
7.51
7.50
7.50
7.49
7.48
7.47
7.44
7.44
7.44
7.43
7.42
7.41
7.40
7.40
7.26
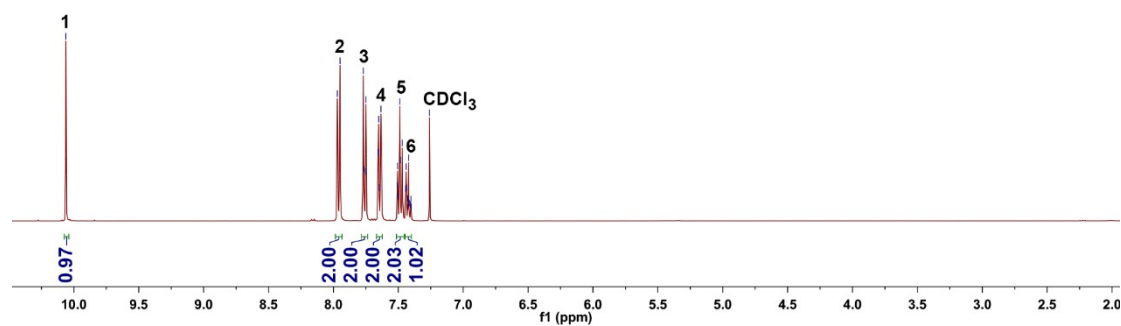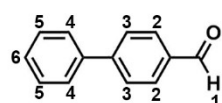
4-phenylbenzaldehyde. White solid. ^{1}H-NMR (400 MHz, CDCl$_3$).
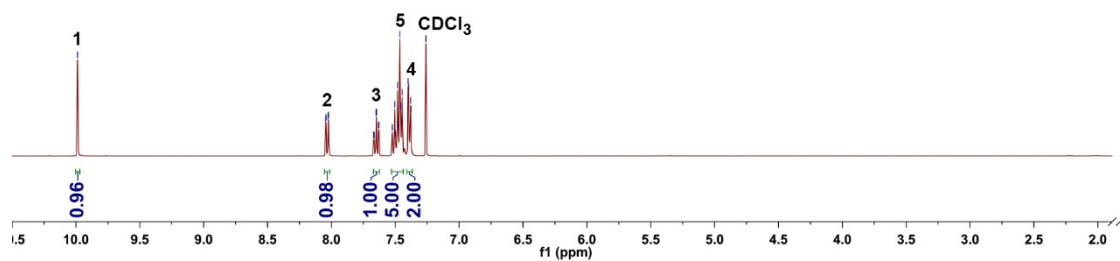
2-phenylbenzaldehyde. White solid. ^{1}H-NMR (400 MHz, CDCl$_3$).

24. Selected bond lengths [Å] and angles [deg] for V-Cd-MOF

V-Cd-MOF			
Cd(1)-O(1)	2.366(4)	Cd(1)-O(1)[#1]	2.366(4)
Cd(1)-N(1)[#2]	2.304(5)	Cd(1)-N(1)[#3]	2.304(5)
Cd(1)-N(2)	2.322(5)	Cd(1)-N(2)[#1]	2.322(5)
V(1)-O(1)	1.614(4)	V(1)-O(13)	1.914(4)
V(1)-O(26)	1.893(4)	V(1)-O(27)	1.913(4)
V(1)-O(28)	1.936(4)	V(2)-O(4)	1.600(4)
V(2)-O(5)	1.815(4)	V(2)-O(13)	2.055(4)
V(2)-O(20)	1.906(4)	V(2)-O(28)	1.900(4)
V(3)-O(5)	1.806(4)	V(3)-O(19)	1.908(4)
V(3)-O(21)	1.887(4)	V(3)-O(31)	1.599(4)
V(3)-O(32)	2.084(4)	V(4)-O(14)	1.977(5)
V(4)-O(20)	1.964(4)	V(4)-O(21)	1.968(4)
V(4)-O(22)	1.982(4)	V(4)-O(30)	1.589(4)
V(5)-O(7)	1.599(4)	V(5)-O(21)	1.915(4)
V(5)-O(22)	1.883(5)	V(5)-O(23)	1.880(4)
V(5)-O(32)	1.920(4)	V(6)-O(9)	1.605(4)
V(6)-O(10)	1.855(4)	V(6)-O(22)	1.911(4)
V(6)-O(23)	2.025(4)	V(6)-O(24)	1.908(4)
V(7)-O(8)	1.597(4)	V(7)-O(23)	1.854(4)
V(7)-O(24)	1.914(4)	V(7)-O(29)	1.950(4)

V(7)-O(33)	1.903(4)	V(8)-O(15)	2.006(4)
V(8)-O(24)	1.968(4)	V(8)-O(25)	1.955(4)
V(8)-O(29)	1.964(4)	V(8)-O(34)	1.602(4)
V(9)-O(10)	1.757(4)	V(9)-O(11)	1.604(4)
V(9)-O(12)	2.047(4)	V(9)-O(14)	1.898(4)
V(9)-O(15)	1.921(4)	V(10)-O(16)	1.746(4)
V(10)-O(17)	1.602(4)	V(10)-O(18)	1.903(4)
V(10)-O(29)	1.879(4)	V(10)-O(33)	2.093(4)
V(11)-O(3)	1.593(4)	V(11)-O(12)	1.909(4)
V(11)-O(15)	1.956(4)	V(11)-O(25)	1.896(4)
V(11)-O(26)	1.825(4)	V(12)-O(2)	1.585(4)
V(12)-O(12)	1.866(4)	V(12)-O(13)	1.828(4)
V(12)-O(14)	1.940(4)	V(12)-O(20)	1.914(4)
V(13)-O(16)	1.898(4)	V(13)-O(25)	1.907(4)
V(13)-O(26)	2.022(4)	V(13)-O(27)	1.907(4)
V(13)-O(35)	1.595(4)	V(14)-O(18)	1.985(4)
V(14)-O(19)	1.960(4)	V(14)-O(27)	1.975(4)
V(14)-O(28)	1.973(4)	V(14)-O(36)	1.603(4)
V(15)-O(6)	1.599(4)	V(15)-O(18)	1.954(4)
V(15)-O(19)	1.909(4)	V(15)-O(32)	1.839(4)
V(15)-O(33)	1.858(4)		
O(1)#1-Cd(1)-O(1)	178.4(2)	N(1)#2-Cd(1)-O(1)	95.85(16)

N(1)$^{\#3}$-Cd(1)-O(1)	83.08(16)	N(1)$^{\#2}$-Cd(1)-N(2)$^{\#1}$	175.90(18)
O(1)-V(1)-O(13)	106.0(2)	O(1)-V(1)-O(27)	110.69(19)
O(13)-V(1)-O(28)	83.06(17)	O(4)-V(2)-O(5)	102.8(2)
O(5)-V(2)-O(20)	91.15(19)	O(28)-V(2)-O(20)	135.76(17)
O(5)-V(3)-O(19)	91.04(18)	O(19)-V(3)-O(32)	78.98(16)
O(32)-V(3)-O(31)	101.7(2)	O(14)-V(4)-O(22)	93.57(18)
O(22)-V(4)-O(21)	77.90(18)	O(21)-V(4)-O(30)	107.0(2)
O(7)-V(5)-O(21)	107.5(2)	O(21)-V(5)-O(32)	82.56(18)
O(32)-V(5)-O(23)	88.51(18)	O(9)-V(6)-O(10)	102.8(2)
O(10)-V(6)-O(22)	88.96(19)	O(22)-V(6)-O(24)	137.64(17)
O(8)-V(7)-O(29)	109.85(19)	O(29)-V(7)-O(24)	79.27(16)
O(24)-V(7)-O(33)	142.81(17)	O(24)-V(8)-O(15)	93.79(16)
O(15)-V(8)-O(34)	103.4(2)	O(34)-V(8)-O(25)	104.01(19)
O(10)-V(9)-O(12)	154.86(18)	O(12)-V(9)-O(14)	77.25(18)
O(14)-V(9)-O(11)	110.3(2)	O(16)-V(10)-O(18)	92.94(18)
O(18)-V(10)-O(33)	76.32(16)	O(33)-V(10)-O(29)	77.13(16)
O(3)-V(11)-O(15)	104.6(2)	O(15)-V(11)-O(12)	80.14(17)
O(12)-V(11)-O(26)	93.44(18)	O(2)-V(12)-O(12)	108.1(2)
O(12)-V(12)-O(20)	142.99(18)	O(20)-V(12)-O(14)	79.11(18)
O(16)-V(13)-O(25)	88.41(17)	O(25)-V(13)-O(27)	136.94(16)
O(27)-V(13)-O(35)	111.7(2)	O(19)-V(14)-O(18)	77.25(17)
O(18)-V(14)-O(28)	147.90(16)	O(28)-V(14)-O(27)	77.53(16)

| O(6)-V(15)-O(18) | 105.3(2) | O(18)-V(15)-O(19) | 79.20(17) |
| O(19)-V(15)-O(32) | 85.40(18) | | |

#1 -X, +Y, 1/2-Z; #2 -X ,-1+Y, 1/2-Z; #3 +X, -1+Y, +Z.

25. Reference

1 Weigend, F.; Ahlrichs, R., Balanced basis sets of split valence, triple zeta valence and quadruple zeta valence quality for H to Rn: Design and assessment of accuracy. *Phys. Chem. Chem. Phys.* **2005**, *7*, 3297-3305.

2 Fukui, K., Formulation of the reaction coordinate. *J. Phys. Chem.* **1970**, *74*, 4161-4163.

3 Peintinger, M. F.; Oliveira, D. V.; Bredow, T., Consistent Gaussian basis sets of triple-zeta valence with polarization quality for solid-state calculations. *J. Comput. Chem.* **2013**, *34*, 451-459.

4 Mammen, M.; Shakhnovich, E. I.; Deutch, J. M.; Whitesides, G. M., Estimating the entropic cost of self-assembly of multiparticle hydrogen-bonded aggregates based on the cyanuric acid·melamine lattice. *J. Org. Chem.* **1998**, *63*, 3821-3830.

5 Li, J.; Huang, X.; Yang, S.; Xu, Y.; Hu, C., Controllable synthesis, characterization, and catalytic properties of three inorganic–organic hybrid copper vanadates in the highly selective oxidation of sulfides and alcohols. *Cryst. Growth Des.* **2015**, *15*, 1907-1914.

6 Shi, F.; Tse, M. K.; Pohl, M.-M.; Brückner, A.; Zhang, S.; Beller, M., Tuning catalytic activity between homogeneous and heterogeneous catalysis: Improved activity and selectivity of free nano-Fe_2O_3 in selective oxidations. *Angew. Chem. Int. Ed.* **2007**, *46*, 8866-8868.

7 Rout, L.; Nath, P.; Punniyamurthy, T., Vanadium-catalyzed selective oxidation of alcohols to aldehydes and ketones with *tert*-butyl hydroperoxide. *Adv. Synth. Catal.* **2007**, *349*, 846-848.

8 Zhu, J.; Kailasam, K.; Fischer, A.; Thomas, A., Supported cobalt oxide nanoparticles as catalyst for aerobic oxidation of alcohols in liquid phase. *ACS Catal.* **2011**, *1*, 342-347.

9 Mei, Q.; Liu, H.; Yang, Y.; Liu, H.; Li, S.; Zhang, P.; Han, B., Base-free aerobic oxidation of alcohols over copper-based complex under ambient condition. *ACS Sustainable Chem. Eng.* **2018**, *6*, 2362-2369.

10 Peng, L.; Zhang, J.; Xue, Z.; Han, B.; Sang, X.; Liu, C.; Yang, G., Highly mesoporous metal–organic framework assembled in a switchable solvent. *Nature Commun.* **2014**, *5*, 4465.

11 Ji, H. B.; Wang, T. T.; Zhang, M. Y.; Chen, Q. L.; Gao, X. N., Green oxidation of alcohols by a reusable nickel catalyst in the presence of molecular oxygen. *React. Kinet. Catal. Lett.* **2007**, *90*, 251-257.